Proceedings of the ASME 2021
Fluids Engineering Division Summer Meeting
FEDSM2021
August 10-12, 2021, Virtual, Online

FEDSM2021-65760

INVESTIGATING THE POTENTIAL DRAG REDUCTION AND THERMAL TRANSPORT IMPROVEMENT IN TEXTURED MICROCHANNELS

Nastaran Rabiei
Northeastern University
Boston, Massachusetts, USA

Grace McDonough
Northeastern University
Boston, Massachusetts, USA

Carlos H. Hidrovo
Northeastern University
Boston, Massachusetts, USA

ABSTRACT

Over the past few decades, microscale duct flow has been the key element for many applications, such as drug delivery and microelectronics cooling. To enhance the performance of such systems and to save more energy, looking for new ways to control the hydrodynamic and thermal characteristics of the microchannel flow has been of great interest lately. The aim of this research is to gain a better understanding of the flow physics within microchannels with microtextured walls. Therefore, a set of numerical study has been conducted on the combined effect of flow and heat transfer for spanwise rectangular trenches. The surface microstructures increase the wetting surface area, which is supposed to increase friction (skin drag). Recirculation produced inside the grooves, on the other hand, aids in increasing main flow slippage and lowering pressure drop along the microchannel. It is also worth noting that recirculation creates a negative pressure difference in the opposite direction of the flow (pressure drag). The geometrical parameters of the trenches have a significant impact on the trade-off between the drag reducing and drag increasing factors in textured microchannel flow, which is addressed in this research. Furthermore, the textures disrupt the thermal boundary layer, which can boost thermal transport through recirculation mixing. However, the stagnant fluid trapped within the grooves has weak convective heat transfer. So far, the results have been promising and a drag reduction of about 25% has been reported for wide trenches at low Reynolds numbers. Thermal transport enhancement is also possible for some tested geometries when the flow has not achieved the thermally fully development.

Keywords: Microtexturing, drag reduction, thermal transport enhancement, skin drag, pressure drag

NOMENCLATURE

a	spacing between the trenches
b	width of the trenches
c	depth of the trenches
w_p	width of the land region
W	width of the equivalent baseline with the same occupying volume
L	length of the microchannel
n	number of the trenches along the channel
$\tau_{w,av}$	average wall shear stress
μ_f	fluid dynamic viscosity
ρ_f	fluid density
ν_f	fluid kinematic viscosity
k_f	fluid conductivity
Re	Reynolds number
D_h	hydraulic diameter
V	velocity
T	temperature
P	pressure
k_s	solid conductivity
ΔP	pressure drop along the channel
A	cross-sectional area
Q	volumetric flow rate
$L_{fd,h}$	entrance length
q''	heat flux
$\overline{Nu}$	average Nusselt number
T_{s_x}	local surface temperature
T_{m_x}	local bulk temperature
h_x	local heat transfer coefficient
$\bar{h}$	average heat transfer coefficient

1. INTRODUCTION

Flow over textured surfaces has always been an interesting topic due to its energy saving benefits in the past few decades. In this case, the flow characteristics can lead to capabilities such as drag reduction and transport augmentation [1]. The idea originates from the denticles on sharks' skin that can help them swim faster while chasing preys [2]. Streamwise riblets on aircrafts can result in 8% drag reduction, which is equivalent to 1.5% less fuel consumption [3]. Different geometries for the textures, such as triangular, rectangular, trapezoidal, and circular (scalloped) have been tested both parallel and perpendicular to the direction of the flow [4]. The geometries with sharp corners experience unfavorable peaks in the shear stress that can increase drag. Spanwise triangular, trapezoidal, and scalloped textures make the cross-sectional area change smoothly along the channel, which make them a good candidate for drag reduction purposes [5]. The geometrical parameters of the trenches that have been considered in the studies are depth, spacing between the textures and the width/curvature of the texture [6]. For instance, triangular riblets can decrease drag in turbulent boundary layer if they are wide and deep enough [7].

Although, most drag reduction studies are focused on large scale external flows in turbulent boundary layer, similar methods can be used in micro length scale. Due to the small length scale of the microchannels they mostly experience low Reynolds numbers and laminar regime. Microchannel flow is inseparable component of microfluidic systems that are widely used in drug delivery [8] and microelectronics cooling [9]. According to Darcy-Weisbach equation, the pressure drop of a laminar fully developed flow is inversely proportional to its hydraulic diameter to the power of four. Therefore, looking for friction reducing methods that can decrease the large pumping power requirement of microchannel flow is encouraging.

The textures are expected to increase the shear forces on the surfaces, since they increase the wetting surface area. For spanwise textures it is not only the friction (skin drag) that results in flow losses. In this case, the formation of the recirculation inside the grooves acts like a cushion [10] and help the fluid in the mainstream to slip at the top of the groove. This phenomenon will decrease the shear forces to some extent. On the other hand, we should be aware of the pressure forces applied in the opposite direction of the flow as the result of recirculation formation [11]. The competition between the pressure drag and skin drag, based on the interaction between the fluid and the solid surface, eventually defines the total drag behavior of the surface. There have been some studies performing optimization studies on the geometrical parameters of the textures to minimize negative effects of the pressure forces and benefit from the slippery effect of the recirculation [12]. In addition to hydrodynamic effects, the thermal characteristics of flow has also been considered in the presence of textures in microchannels. For example, the numerical studies on channels with fan-shaped ribs have not shown drag reduction compared to the baseline. However, thermal transport can be enhanced when the ratio of the rib's height to the distance between the parallel sides is increased [6,13]. The offset and aligned patterns are also studied and the results show that the former experience less pressure losses, but the latter shows higher thermal transport [14].

With many studies showing drag reduction results when using textured channels compared to the smooth ones, one should be careful about choosing the correct reference for comparison. The results of a study [15] has shown that the correct baseline channel for comparing the drag reduction results with, should maintain the same occupying volume as the textured channel. Therefore, the drag reduction results of some studies may have been misinterpreted due to the failure in considering a correct reference baseline channel.

In this work, the effect of rectangular textures on the hydrodynamics and thermal characteristics of microchannel flow has been studied. Therefore, 2D numerical simulations have been conducted on 30 textured microchannels at Reynolds numbers of 5, 50, 200 and 500 using COMSOL Multiphysics. The geometrical properties of the textures are calculated such that they all maintain the same volume. The equivalent baseline for all the cases will be two parallel plates with the distance of $100\,\mu m$ between them. The Poiseuille number is the representative of the hydraulic resistance of the flow and average Nusselt number is calculated to quantify the thermal transport of the flow. Based on the flow characteristics, the different concepts of locally fully development and globally fully development have been introduced. The calculation of the Poiseuille number is done for the globally fully developed flow for all the textured microchannels. The results have shown that drag reduction is possible for wide textures at lower Reynolds numbers.

2. MATERIALS AND METHODS

2.1 Computational Domain and Geometrical Parameters

The computational domain in Figure 1(a) shows flow over spanwise rectangular textures in a 2D microchannel. Due to symmetry of the microchannel flow and its geometry, half of the microchannels are simulated to avoid the unnecessary computational load. The microchannel is embedded in PDMS (Polydimethylsiloxane) and there is a heater on the side, parallel to the main channel flow. Water has been used as the working fluid inside the microchannels. The important geometrical parameters of the textures are also labeled in Figure 1(b), which are spacing between the trenches (a), width of the trench (b), depth of the trench (c), width of the land region (w_p) and width of the equivalent baseline with the same occupying volume (W). All the microchannels (textured and baseline) are designed such that they all have the same volume. Therefore, the pressure drop along different microchannels will be independent from their hydraulic diameter and cross-sectional area, and the comparison of the drag behavior will be valid [15]. Equation (1) shows the relation between the geometrical parameters of the textured microchannels to maintain the same volume, where L is the length of the microchannel and n is the number of trenches:

$$WL = w_p L + 2cb \ ; \ L = n(a + b) \tag{1}$$

The effect of each geometrical parameter of the trench (a, b & c) on the flow and heat transfer has been individually studied by keeping other parameters at the constant value of 20 μm. The ranges in which the parameters a, b & c change, are 5-780 μm, 5-780 μm and 5-95 μm, respectively. Equal length of microchannels (1600 μm) has been considered for the Poiseuille number (Po) calculation. The width of the baseline (W) is 100 μm for all cases. By substituting values for the parameters, a, b, c, n and W, the value of w_p for each microchannel is calculated using equation (1).

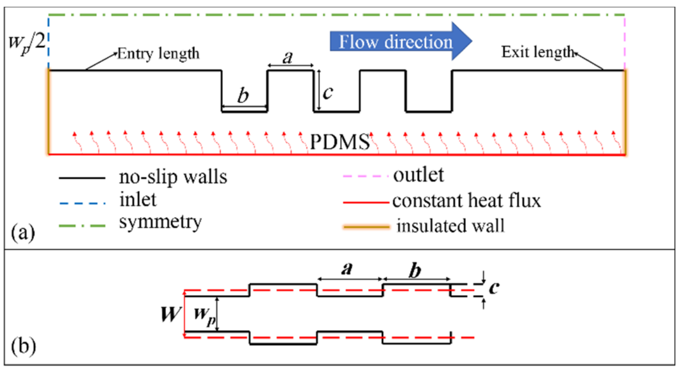

Figure 1. (A) THE SCHEMATIC OF THE COMPUTATIONAL DOMAIN WITH BOUNDARY CONDITIONS, (B) THE IMPORTANT GEOMETRICAL PARAMETERS OF THE TEXTURED MICROCHANNEL

2.2 Governing Equations and Boundary Conditions

The continuity, momentum and energy equations are solved for the 2D solid-fluid conjugate model. The following governing equations are used in the simulations, equations (2-5):

Continuity:

$$\nabla.(\rho_f \boldsymbol{u}) = 0 \tag{2}$$

Momentum:

$$\nabla(\rho_f \boldsymbol{u}.\boldsymbol{u}) = -\nabla p + \nabla.[\mu_f(\nabla \boldsymbol{u} + (\nabla \boldsymbol{u})^T)] \tag{3}$$

Energy:

For Fluid: $$\nabla\left(\rho_f c_{p_f} \boldsymbol{u} T\right) = \nabla.\left(k_f \nabla T\right) + \mu_f(\nabla \boldsymbol{u} + (\nabla \boldsymbol{u})^T) \tag{4}$$

For Solid: $$\nabla.(-k_s \nabla T) = 0 \tag{5}$$

where the parameters denoted with the subscript "f" and "s" are the properties of the fluid and solid, respectively. The fluid properties are considered temperature dependent, while the conductivity of PDMS is defined constant ($k_s = 0.16 \frac{W}{m.K}$). Since formation of instabilities is possible for flows inside textured channels, modified Reynolds number is defined based on friction velocity to recognize the potential of occurrence of instabilities in internal flow [16]. In equation (6), W is the width of the channel and $\tau_{w,av}$ is the average wall shear stress. The studies have shown that for Re_τ smaller than 40-60, the flow will not experience instabilities. Therefore, by considering this criterion for the textured microchannels at four Reynolds numbers of 5, 50, 200 and 500, performing the simulations in steady state and two dimensional is a valid approximation.

$$Re_\tau = \frac{W/2}{\nu_f} \sqrt{\frac{\tau_{w,av}}{\rho_f}} \tag{6}$$

The boundary conditions of the computational domain are depicted in Figure 1(a). At the inlet of the microchannel, uniform velocity profile and temperature has been applied. The inlet velocity can be calculated based on the desired Reynolds number and the thermophysical parameters of the fluid at 20°C given in equation (7). D_h is the hydraulic diameter of the microchannels, which is 200 μm for all and the same value of the hydraulic diameter of the baseline ($D_h = 2W$).

$$@\ x = 0; \begin{cases} V = V_i \ , \ V_i = \dfrac{Re\, \mu_{f,i}}{\rho_{f,i} D_h} \\ T = T_i \end{cases} \tag{7}$$

Constant ambient pressure has been applied as the boundary condition at the outlet of the microchannel. Also, the temperature gradient is neglected at the outlet, which means that the only heat transfer mode that is occurring across this boundary is convection. The outlet boundary conditions are summarized in equation (8):

$$@x = L; \begin{cases} P_{gauge} = 0 \\ \dfrac{\partial T_f}{\partial x} = 0 \end{cases} \tag{8}$$

The symmetry boundary condition for both momentum and energy equations are considered, since there are no temperature and velocity gradient normal to the centerline of the microchannel, equation (9):

$$@y = \frac{wp}{2}; \begin{cases} \dfrac{\partial u_f}{\partial y} = 0 \\ \dfrac{\partial T_f}{\partial y} = 0 \end{cases} \tag{9}$$

Finally, the constant heat flux at the lower edge of PDMS is applied using equation (10). It should be noted that for all simulations the heater is placed 40 μm away from the bottom edge of the microchannel trenches.

$$@y = -c - 40; \ -k_s \frac{\partial T_s}{\partial y} = 1000 \frac{W}{m^2} \tag{10}$$

The inner boundaries of the microchannel that are shown as black lines in Figure 1(a) have the no-slip boundary condition. The two orange vertical boundaries at the end of the PDMS are insulated walls to eliminate the heat transfer from the sides to the surrounding.

To characterize the hydrodynamic and thermal behavior of the microchannels, the Poiseuille number and the average Nusselt number are used. Due to the Darcy-Weisbach equation for laminar fully developed flow, the Poiseuille number is the representative of the hydraulic resistance. For a microchannel flow with length of L, hydraulic diameter of D_h, cross-sectional area of A, the Poiseuille number is calculated by equation (11):

$$Po = \frac{2\,\Delta P\,A\,D_h^2}{\mu\,Q\,L} \tag{11}$$

where the parameters ΔP, μ and Q are respectively the pressure drop, dynamic viscosity and flow rate of the fluid. Since the geometrical parameters A, D_h, L are the same for all microchannels and the variation of μ in different cases is less than 1%, that can be neglected, the Poiseuille number is a well-chosen parameter to compare the pressure drop along different microchannels at a specific flow rate.

Equation (10) is valid for fully developed flow and it is important to study the effect of textures on the mechanism of fulfilling fully development. The profile of centerline velocity along the microchannels has been depicted for all the cases. For instance, Figure 2 shows the centerline velocity profile of three textured microchannels with different values of b at Reynolds number of 5. It can be noticed that due to the cross-sectional variation along the textured microchannels, the flow can never reach locally fully development as conventionally defined. However, we can see at some point along the channel the wavy behavior of the centerline velocity repeats itself with exactly the same amplitude and wavelength. In other words, one can infer that for the textured geometries reaching globally fully development can be defined, while the term locally fully development is not applicable. In this case, globally fully development is fulfilled when the flow field shows repeating patterns. This behavior is consistent with the periodic pattern of the trenches along the microchannel.

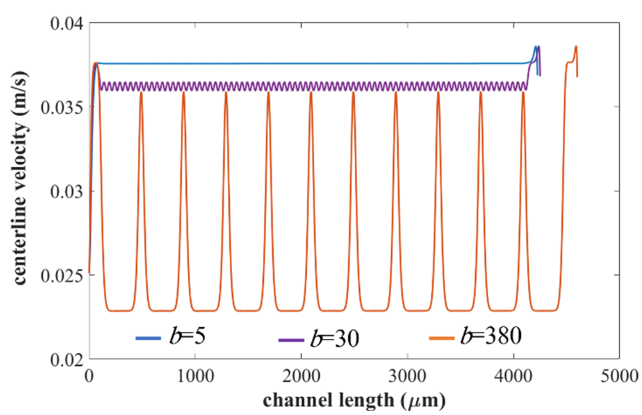

Figure 2. CENTERLINE VELOCITY PROFILE OF THREE TEXTURED MICROCHANNELS WITH a=20μm, c=20μm AND DIFFERENT VALUES OF b; BLUE LINE: b=5μm, PURPLE LINE: b=30μm, ORANGE LINE: b=380μm.

As a result, the entrance length of the textured microchannels can be reported based on the number of periods, that consists of a groove and land region. Table 1 shows the entrance length of the cases in which parameter b is changing and parameters a and c are 20 μm. Under each Reynolds number, the first column shows the number of the period where globally fully development is achieved, and the second column is the entrance length in microns. As can be seen the value of entrance length from centerline velocity plots is different from what is calculated from theory for a smooth channel in the last row ($L_{fd,h} \approx 0.06 Re_{D_h} D_h$). Depending on the length of one period, summation of parameters a and b, the entrance length of a textured channel can increase, or decrease compared to the theoretical value.

Table 1. SUMMARY OF THE ENTRANCE LENGTH FOR THE TEXTURED MICROCHANNELS IN WHICH PARAMETER b IS VARIABLE, FOR DIFFERENT REYNOLDS NUMBERS.

	Re=5		*Re=50*		*Re=200*		*Re=500*	
b (μm)	*No.*	L(μm)	*No.*	L(μm)	*No.*	L(μm)	*No.*	L(μm)
5	3	175	7	275	27	775	60	1600
12	2	164	3	196	19	708	43	1476
20	2	180	3	220	14	660	33	1420
30	1	150	3	250	11	650	25	1350
60	1	180	2	260	7	660	15	1300
80	1	200	2	300	6	700	13	1400
140	1	260	2	420	3	580	9	1540
180	1	300	2	500	4	900	7	1500
380	1	500	1	500	3	1300	5	2100
780	1	900	1	900	2	1700	3	2500
$L_{ent,th}$ (μm)	60		600		2400		6000	

It should also be noted that, an entry and exit length of 100 μm is considered in the computational domain to make the solution robust to the inlet and exit effects. The investigations showed that changing the length of entry and exit length causes less than 1% variation in the Poiseuille number value of the globally fully developed flow inside textured microchannels.

When a constant heat flux q'' is applied at the wall of the channel, the average Nusselt number $\overline{Nu}$ is calculated using equation (11):

$$\begin{cases} h_x = \dfrac{q''}{(T_s - T_m)|_x} \\ T_{m_x} = \dfrac{\int \rho_f\, u\, c_{p_f} T\, dA\,|_x}{\int \rho_f\, u\, c_{p_f}\, dA\,|_x} \\ \bar{h} = \frac{1}{A}\int h_x dA \end{cases} \Rightarrow \quad \overline{Nu} = \frac{\bar{h} D_h}{k_f} \tag{11}$$

In equation (11), the parameters T_{s_x}, T_{m_x}, u, h_x, $\bar{h}$ and k_f show local surface temperature, local bulk temperature, velocity, local heat transfer coefficient, average heat transfer coefficient and conductivity of the fluid. The calculation of the Nusselt number can help provide a better understanding of how much of the heat flux that is conducted through the wall of the microchannel is conveyed by the moving fluid through convection.

2.3 Mesh Resolution Study

Mesh resolution studies have been conducted to make sure that the solution is independent from the elements used for meshing the computational domain. Figure 3 depicts a section of the fluid region that is meshed using structured Mapped grid. The element ratio is adjusted such that the density of the elements gets higher near the walls and sharp corners. This is essential to capture the phenomena in these critical locations. Figure 4 shows the Poiseuille number value of the baseline and two other textured microchannels with respect to the total number of elements. Due to the results, with the average element size of 0.2 μm in y direction and 0.5 μm in x direction, the Poiseuille number for baseline shows less than 1% error compared to its theoretical value, which is 96 for flow between two parallel plates. Using the same dimensions for the textured microchannels, the variation of their Poiseuille number will also be less than 1%.

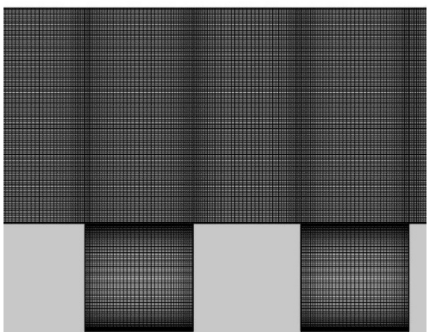

Figure 3. MAPPED GRID USED TO MESH THE COMPUTATIONAL DOMAIN OF TEXTURED MICROCHANNELS

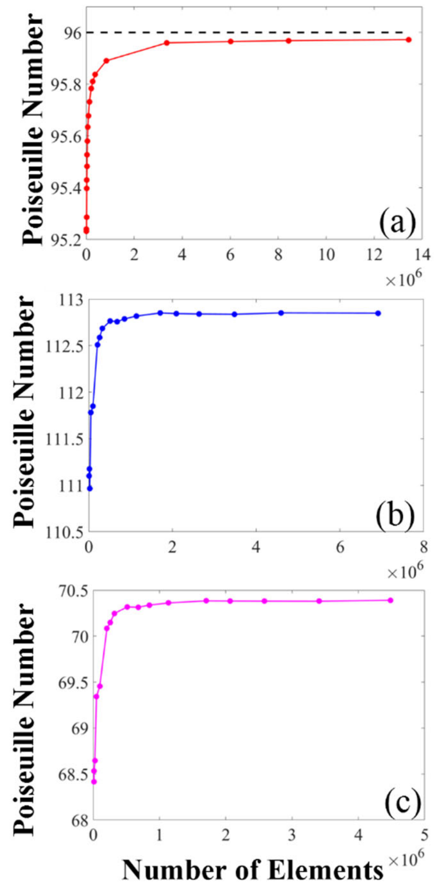

Figure 4. MESH RESOLUTION STUDY FOR 2D MICROCHANNEL FLOW SIMULATIONS BASED ON THE POISEUILLE NUMBER CALCULATION, (A) BASELINE, (B) TEXTURED CHANNEL WITH a=c=20μm AND b=5μm, (C) TEXTURED CHANNEL WITH a=c=20μm AND b=780μm

3 RESULTS AND DISCUSSION

3.1 Hydrodynamic Results

The results of Poiseuille number and flow streamlines with variation of width of the trench (*b*) for four Reynolds numbers are illustrated respectively in Figure 5 and Figure 6. At a specific Reynolds number, before the Poiseuille number reaches its maximum value, increasing the width of the trench makes the recirculation larger, which results in increase of pressure forces at the vertical walls. On the other hand, as the size of the recirculation increases, the shear forces at the bottom wall of the trenches increase. Hence, larger shear forces in the direction of flow outweigh the shear forces in the opposite direction of flow on the land region. For instance, the variation of pressure and shear forces is shown in Figure 7 for Reynolds number of 5. The results for other Reynolds numbers show similar behaviors. Although, two different behaviors are observed for pressure forces and shear forces, the pressure forces dominate the behavior of the Poiseuille number showing an overall increase. As the width of the trench (*b)* further increases, the recirculation gets more susceptible to collapsing. At some point, the main flow streamlines will start to bend inside the trench and collapse the recirculation. Therefore, the recirculation

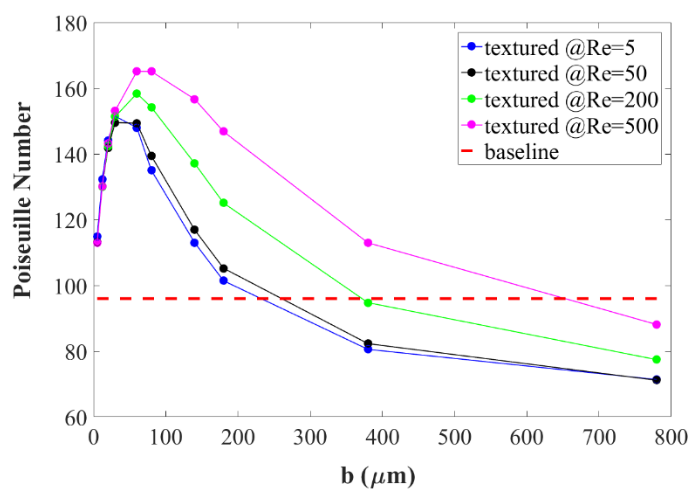

Figure 5. VARIATION OF THE POISEUILLE NUMBER WITH PARAMETER *b*, WHICH IS THE WIDTH OF THE TRENCHES AT REYNOLDS NUMBERS OF 5, 50, 200 AND 500

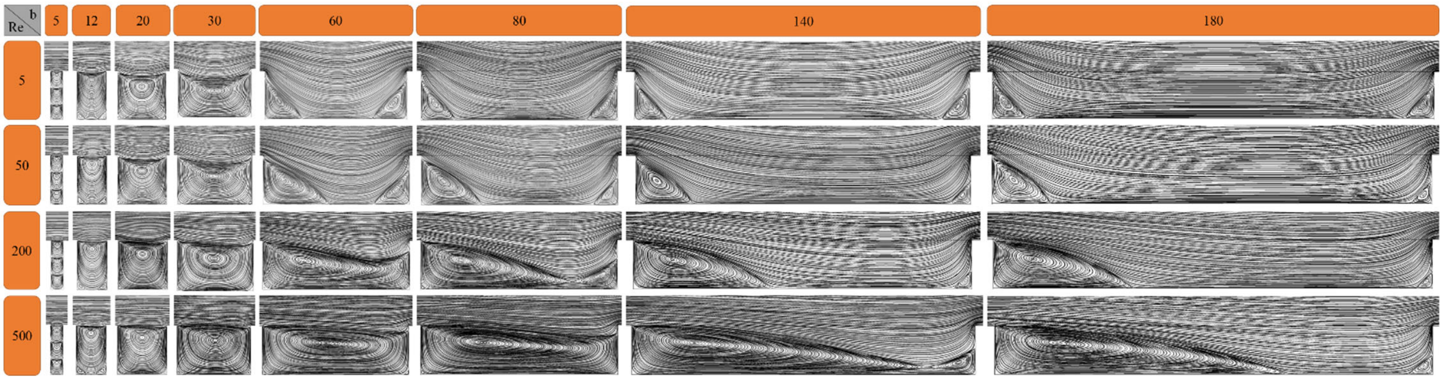

Figure 6. STREAMLINES OF FLOW INSIDE A TEXTURED MICROCHANNEL WITH DIFFERENT VALUES OF *b*. FOR ALL THE TRENCHES SHOWN THE VALUES OF *a* AND *c* ARE 20 MICRONS.

divides into two parts at the corners. At the brink of the collapse of the recirculation, the pressure forces reach their maximum value and that is the point where the flow experiences the least shear forces. As the streamlines start to bend inside the trench and touch the bottom surface, the trend of pressure forces and shear forces change direction. Now that the recirculation has collapsed, negative pressure forces decrease with increase of *b*, and because streamlines touch the bottom surface, the shear forces in the opposite direction of the flow start to increase.

For wide trenches, the recirculation at the left-hand side corner alleviates the shear force increase to some extent. Consequently, the increase of the shear force is not able to overcome the decrease in the pressure forces, and for some cases, when *b* is equal to 380 & 780, the Poiseuille number of the textured channel becomes smaller than the baseline. It can also be noticed that as the Reynolds number increases the Poiseuille number for the cases that experience drag reduction, increases, and gets closer to or even larger than the baseline Poiseuille number.

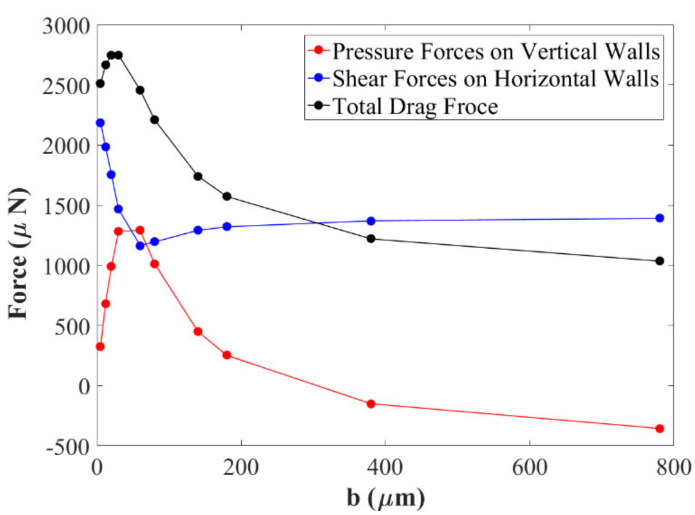

Figure 7. FORCES AFFECTING THE DRAG BEHAVIOR OF THE TEXTURED MICROCHANNEL FLOW HAVING DIFFERENT VALUES FOR PARAMETER *b* AT RE=5

Figure 8 shows the effect of depth of the trenches (c) on the Poiseuille number behavior. Despite the previous observations that pressure forces are dominant in the trend of the Poiseuille number when changing the width of the trenches (b), the variation of the Poiseuille number with the depth of the trenches (c) is shear force dominated. Based on Figure 9, as the trenches get deeper, both the shear and pressure forces increase. Due to the definition of shear stress being the ratio of velocity variation to the dimension variation perpendicular to the flow direction, as the trenches get deeper and the width of the land region w_p decreases, the shear stress and shear force increase. Moreover, as the trenches get deeper, two or three recirculation forming at the top of each other inside the groove result in the increase of pressure force. Since there is a relatively large dead volume of liquid trapped inside the deep trenches, it is suggested to measure the effective depth of the trenches from the simulations and use that in the calculations of hydraulic diameter and the Poiseuille number. By doing so, the values of the Poiseuille number for very deep trenches, e.g. c= 65, 75, 85 & 95 µm, will decrease by nearly 80%.

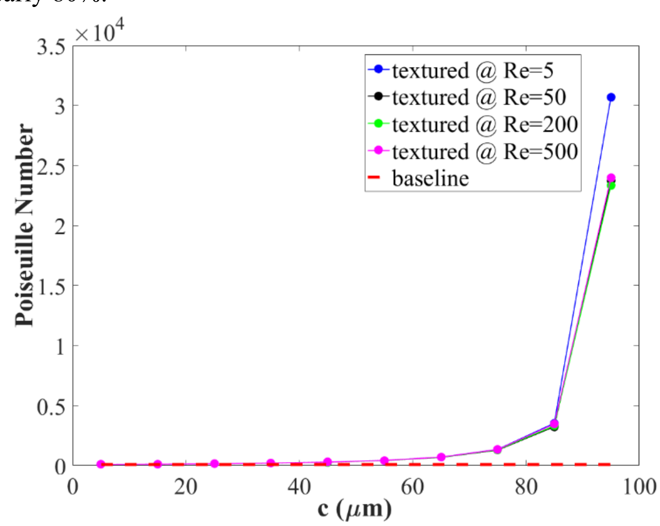

Figure 8. VARIATION OF THE POISEUILLE NUMBER WITH PARAMETER *c*, WHICH IS THE WIDTH OF THE TRENCHES AT REYNOLDS NUMBERS OF 5, 50, 200 AND 500

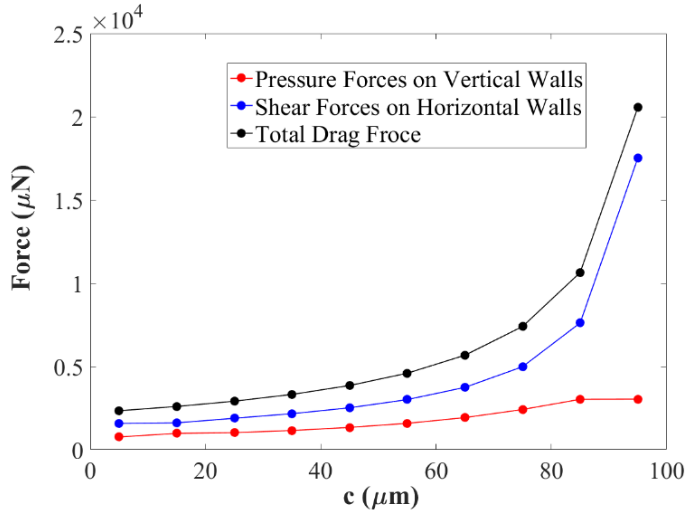

Figure 9. FORCES AFFECTING THE DRAG BEHAVIOR OF THE TEXTURED MICROCHANNEL FLOW HAVING DIFFERENT VALUES FOR PARAMETER *c* AT RE=5

Figure 10 and Figure 11 show the plots of Poiseuille number and pressure/shear forces with respect to the spacing between the trenches (*a*). It is expected that as the land region gets wider, the opposing shear forces increase and result in higher drag forces. Looking closely at the induced pressure forces at the vertical walls of the trenches and shear forces at the horizontal walls proves otherwise. As the spacing between the trenches increases between the trenches, the pressure forces and shear forces have opposite behaviors, decreasing and increasing, respectively. Eventually the total drag force will decrease with the increase of *a*. This is indicative of the fact that the effect of pressure forces on vertical walls is dominant over the shear forces on the horizontal walls. The decreasing trend of the pressure forces on the vertical walls as *a* increases can

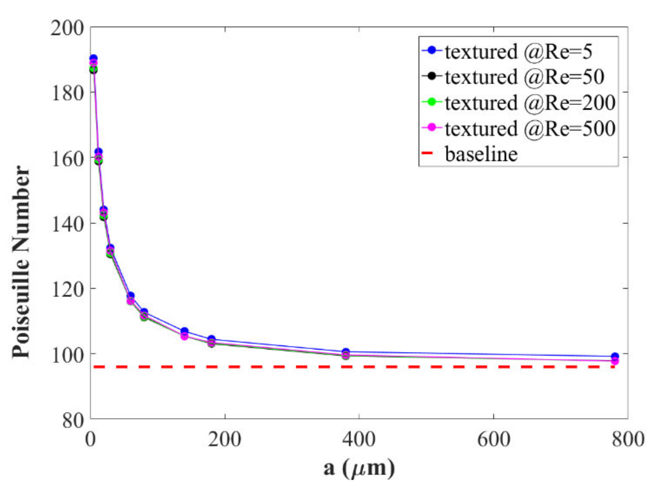

Figure 10. VARIATION OF THE POISEUILLE NUMBER WITH PARAMETER A, WHICH IS THE WIDTH OF THE TRENCHES AT REYNOLDS NUMBERS OF 5, 50, 200 AND 500

partially be attributed to the fact that the number of the trenches decrease for a given length of the microchannel, and the negative effect of the pressure forces are alleviated. With the trend in this plot, if the value of *a* goes to infinity, the Poiseuille number of the textured channel will show an asymptotic behavior around the baseline value (96). It can also the noticed that the Poiseuille number behavior with variation of *a* does not depend on the Reynolds number.

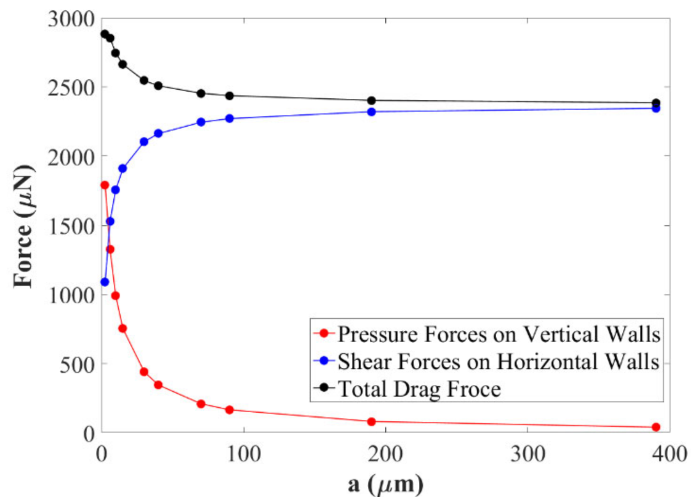

Figure 11. FORCES AFFECTING THE DRAG BEHAVIOR OF THE TEXTURED MICROCHANNEL FLOW HAVING DIFFERENT VALUES FOR PARAMETER *a* AT RE=5

3.2 Thermal Results

The average Nusselt number with respect to the variation of parameters *a*, *b* and *c* individually is shown in Figure 12(a-c). For all the cases, the distance between the heaters and the bottom wall of the trenches is less than the distance between the heater and the land region (spacing between the trenches) of the textured channel. Hence, less conductive resistance is experienced in the former and larger portion of the heat rate passes through the bottom of the grooves. However, the stagnant fluid trapped inside the groove does not help with the convection and cannot convey the heat flux to the upper layers of fluid. As a result, the wall temperature increases and the temperature difference between the bulk and wall temperature will be higher than that of in the land region.

By briefly looking at the figures, we realize that the variation of the average Nusselt number with *b* and *a* has the opposite trend compared to the variation of the Poiseuille number with these parameters. From Figure 12(a), it is inferred that for a specific value of *b* in which the recirculation is at its strongest position (minimum Poiseuille number), the Nusselt number has the minimum value. This can be attributed to poor convection in the recirculation area. As the width of the trench increases and the streamlines bend inside the groove and touch the bottom surface, the convection thermal transport will be enhanced. Figure 12(b), shows that the average Nusselt number is higher for deeper trenches. This can be due to transfer of more heat rate

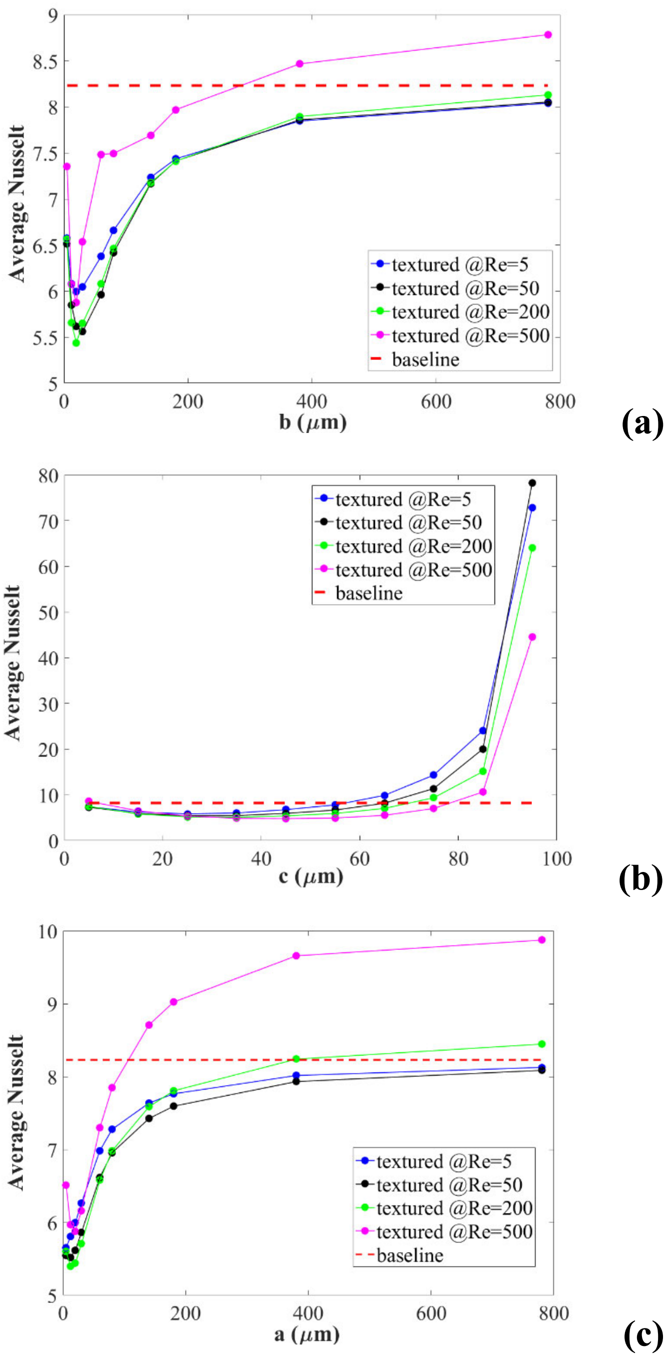

Figure 12. VARIATION OF AVERAGE NUSSELT NUMBER WITH PARAMETERS *b*, *c* AND *a*, RESPECTIVELY AT REYNOLDS NUMBERS OF 5, 50, 200 AND 500.

to the fluid through the vertical walls, as the trenches get deeper. From Figure 12(c), it seems that increasing the land region *a*, diminishes the negative poor convective thermal transport through the recirculation areas of the grooves. Therefore, more portion of heat rate will be transferred through the land region with the convection mechanism. It should also be noted that for Reynolds number of 500 in Figure 12(a) and Figure 12(c), the values of Nusselt number are higher compared to other Reynolds numbers. This is due to the fact that at this Reynolds number the flow has not reached globally thermally fully development (similar terminology that was introduced in the previous section about globally hydrodynamic fully development), therefore showing thermal transport enhancement. So far, we know that the textures tested in this study do not enhance thermal transport compared to the baseline (Nusselt number for flow between two parallel plates with constant heat flux at walls is 8.2) when the flow is thermally fully developed. The effect of geometrical parameters of the textures on the thermal transport characteristics is still ongoing and needs further investigations.

4 CONCLUSION

The effect of geometrical parameters of the rectangular textures at Reynolds numbers of 5, 50, 200 and 500 is investigated. At Reynolds number of 5 and 50, wide grooves have shown about 25% drag reduction compared to a smooth channel. The results of thermal transport still need further investigations, however, for globally thermally fully developed flow no thermal transport enhancement has been reported.

ACKNOWLEDGEMENTS

We appreciate our funding source, NSF CBET award number 1705958.

REFERENCES

1. Scholle, M., Rund, A. & Aksel, N. "*Drag reduction and improvement of material transport in creeping films*" *Arch. Appl. Mech.* Vol. **75** (2006): pp. 93–112.
2. Bhushan, B. "*Biomimetics: Lessons from Nature - an overview*" *Philos. Trans. R. Soc. A Math. Phys. Eng. Sci.* Vol. **367** (2009): pp. 1445–1486.
3. Ball, P. "*Engineering Shark skin and other solutions*" *Nature* Vol. **400** (1999): pp. 507–509.
4. Jung, Y. & Bhushan, B. "*Biomimetic Structures for Fluid Drag Reduction in Laminar and Turbulent Flows*" *J. Phys. Condens. Matter* Vol. **22** (2010): pp. 35104.
5. Rawool, A. S., Mitra, S. K. & Kandlikar, S. G. "*Numerical simulation of flow through microchannels with designed roughness*" *Microfluid. Nanofluidics* Vol. **2** (2006): pp. 215–221.
6. Chai, L., Xia, G. D. & Wang, H. S. "*Parametric study on thermal and hydraulic characteristics of laminar flow in microchannel heat sink with fan-shaped ribs on sidewalls – Part 2: Pressure drop*" *Int. J. Heat Mass Transf.* Vol. **97** (2016): pp. 1081–1090.
7. Walsh, M. J. "*Riblets as a Viscous Drag Reduction Technique*" *AIAA J.* Vol. **21** (1983): pp. 485–486.
8. Liu, D., Zhang, H., Fontana, F., Hirvonen, T. J. & Santos, H. "*Microfluidic-Assisted Fabrication of Carriers for Controlled Drug Delivery*" *Lab Chip* (2017): pp. 1856–1883.
9. Hidrovo, C. & Kenneth, G. "*Active Microfluidic Cooling of Integrated Circuits*" in *Electrical, Optical and Thermal Interconnections for 3D Integrated Systems* (2008): pp. 293–330.

10. Raayai-Ardakani, S. & McKinley, G. H. "*Drag reduction using wrinkled surfaces in high Reynolds number laminar boundary layer flows*" *Phys. Fluids* Vol. **29**(2017): 93605.
11. Tirandazi, P. & Hidrovo, C. H. "*Study of drag reduction using periodic spanwise grooves on incompressible viscous laminar flows*" *Phys. Rev. Fluids* Vol. **5**, 64102.
12. Friedmann, E. (2010) "*The Optimal Shape of Riblets in the Viscous Sublayer*" *J. Math. Fluid Mech.* Vol. **12** (2020): pp. 243–265.
13. Chai, L., Xia, G. D. & Wang, H. S. "*Parametric study on thermal and hydraulic characteristics of laminar flow in microchannel heat sink with fan-shaped ribs on sidewalls – Part 1: Heat transfer*" *Int. J. Heat Mass Transf.* Vol. **97** (2016): pp. 1069–1080.
14. Kharati-Koopaee, M. & Zare, M. "*Effect of aligned and offset roughness patterns on the fluid flow and heat transfer within microchannels consist of sinusoidal structured roughness*" *Int. J. Therm. Sci.* Vol. **90** (2015): pp. 9–23.
15. Daschiel, G., Peric, M., Jovanovic, J. & Delgado, A. "*The holy grail of microfluidics: Sub-laminar drag by layout of periodically embedded microgrooves*" *Microfluid. Nanofluidics* Vol. **15** (2013).
16. Kandlikar, S. G. "*Exploring Roughness Effect on Laminar Internal Flow–Are We Ready for Change?*" *Nanoscale Microscale Thermophys. Eng.* Vol. **12** (2008) : pp. 61–82.